

ISOPHOT Serendipity Survey observations of interstellar clouds^{*}

I. Detection of the Coldest Cores in Chamaeleon

L.V. Tóth^{1,2}, S. Hotzel¹, O. Krause¹, K. Lehtinen³, D. Lemke¹, K. Mattila³, M. Stickel¹, and R.J. Laureijs⁴

¹ Max-Planck-Institut für Astronomie, Königstuhl 17, 69117 Heidelberg, Germany

² Loránd Eötvös University, Department of Astronomy, Pázmány Péter sétány 1/a, 1117 Budapest, Hungary

³ Helsinki University Observatory, P.O. Box 14, 00014 University of Helsinki, Finland

⁴ ISO Science Operations Centre, Astrophysics Division of ESA, Villafranca, P.O. Box 50727, 28080 Madrid, Spain

Received 24 May 2000 / Accepted 6 October 2000

Abstract. ISOPHOT Serendipity Survey (ISOSS) observations at 170 μm reveal cold dust clouds in the nearby star forming region Chamaeleon. The distribution of the ISOSS/IRAS based $T(I_{170}/I_{100})$ colour temperature have been studied in a nearby low-mass star forming region. $T(I_{170}/I_{100})$ separates the obscured and intercloud regions as seen from a comparison to optical extinction data. The interstellar medium in Chamaeleon-Musca appears to be cold with dust colour temperatures of ≈ 16.3 K for intercloud regions, and ≤ 14.5 K for obscured clouds. The cold clouds account for 3% of the area. ISOSS found 9 very cold cores with colour temperatures as low as $T_{\text{dust}} \lesssim 12.5$ K in an $11^\circ \times 8^\circ$ sized region. All C^{18}O cores of the Chamaeleon main clouds which were crossed by ISOSS slews were also detected. Of these 11 (73%) are cold with $T_{\text{dust}} \leq 15$ K, 6 (40%) are associated with very cold cores. The very cold cores have high gas column densities, $N(\text{H}_2) > 10^{21} \text{ cm}^{-2}$, and 7 out of 9 have low gas kinetic temperatures as indicated by $T_{\text{ex}}(\text{C}^{18}\text{O}) \approx 8$ K. The physical parameters of the very cold cores agree with the results of radiative transfer calculations of a spherical model cloud heated from outside by one third of the the solar neighbourhood ISRF intensity. A check of the photometric calibration of ISOSS against ISOPHOT AOT PHT22 maps and DIRBE interpolated 170 μm values showed an agreement of $\pm 10\%$ and $\pm 20\%$, respectively. We expect to discover in total more than 100 very cold cores in the Galaxy by ISOSS.

Key words: ISM: clouds – ISM: dust, extinction – ISM: individual objects: Chamaeleon clouds – ISM: molecules – infrared: ISM: continuum – surveys

Send offprint requests to: L.V. Tóth

^{*} Based on observations with ISO, an ESA project with instruments funded by ESA Member States (especially the PI countries: France, Germany, the Netherlands and the United Kingdom) and with the participation of ISAS and NASA. Members of the Consortium on the ISOPHOT Serendipity Survey (CISS) are MPA Heidelberg, ESA ISO SOC Villafranca, AIP Potsdam, IPAC Pasadena, Imperial College London.

1. Introduction

The ISOPHOT Serendipity Survey (ISOSS) is the first large scale survey in the 200 μm band. It has mapped a substantial fraction of the sky with 3' wide strip scans while ISO was slewing between pointed observations (Lemke et al. 1996; Bogun et al. 1996; Kessler et al. 1996). Besides detecting large numbers of point sources, which in most cases at higher galactic latitudes are galaxies (Stickel et al. 1998a,b), a lot of ISOSS slew measurements show extended FIR sources such as interstellar clouds and cloud cores in the nearest star forming regions. To a large extent, these galactic sources have not yet been observed beyond the IRAS 100 μm limit. The sample we may obtain analysing the complete ISOSS database is much larger than any of the previous FIR air-born (see eg. Keene 1981), sub-mm range ground-based (see eg. Launhardt et al. 1997), or balloon (see eg. Ristorcelli et al. 1998) measurements.

For sources larger than the beamsize ($\approx 2'$ for ISOSS), the measured intensity directly reflects the 170 μm surface brightness of the object, after the background emission has been determined and subtracted. For all common dust models, the 170 μm surface brightness is a measure of a combination of column density and temperature of the big grain component, as long as the source is not optically thick. Since the properties of this dust are relatively well known, one other FIR wavelength is sufficient for an estimation of the dust temperature. The best data set for a comparison with ISOSS is the IRAS Sky Survey Atlas (ISSA, Wheelock et al. 1994) at 100 μm . A combination can provide several parameters that characterize galactic molecular clouds and cold cloud cores.

Model calculations for diffuse clouds predict silicate dust grain temperatures down to ≈ 15 K (Draine & Lee 1984). Analysis of COBE data has proved the presence of a widespread 15 K cold dust component in addition to the overall 17.5 K cirrus component in the Milky Way (Lagache et al. 1998). Due to COBE's low resolution, a spatial distinction between the two components could not be given. It is however expected that dust in diffuse clouds is slightly colder than dust of the surrounding interstellar medium (ISM), due to the attenuation of the interstellar radiation field (ISRF). In regions totally shielded from

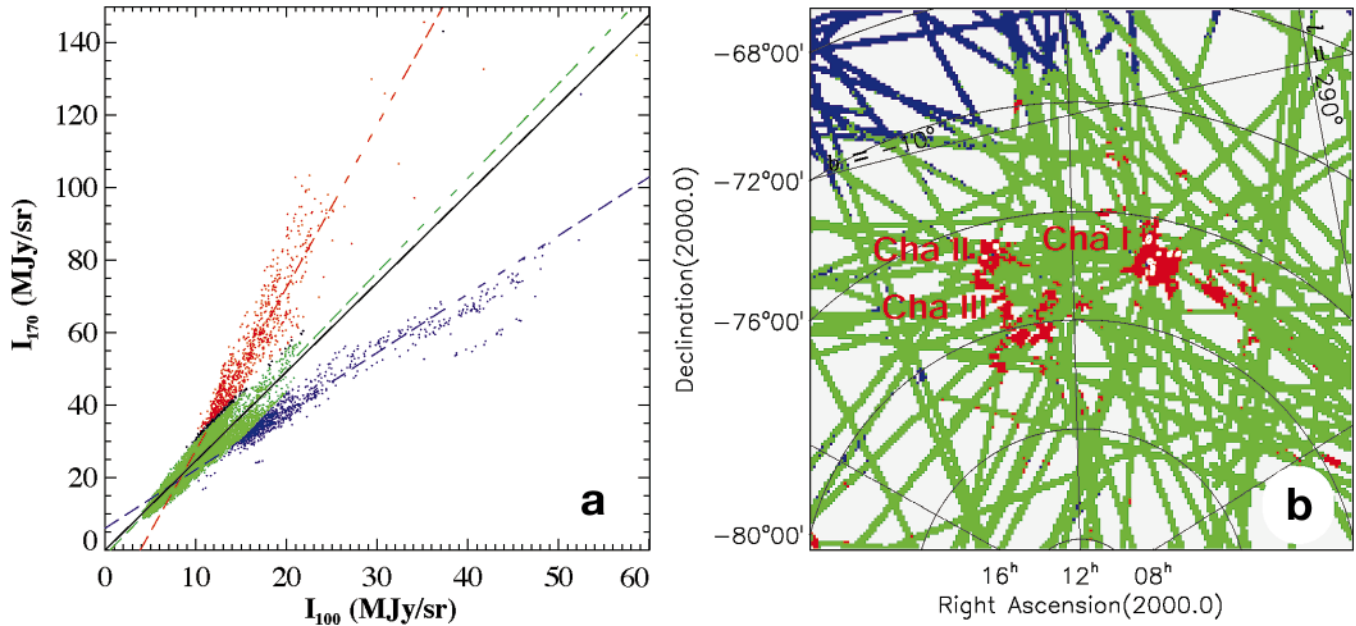


Fig. 1. **a** $I_{170} - I_{100}$ correlation plot for the Chamaeleon-Musca region. Surface brightnesses have been read out from a $20^\circ \times 20^\circ$ ISOSS slewmap and the ISSA maps at the slew sample positions. The linear correlation line $I_{170} = 2.46 \times I_{100}$ is a least-squares fit for the whole field (continuous line). It has been used to differentiate between cold and warm regions. Data points with $I_{170} > 5 \text{ MJy sr}^{-1}$ above or below the line belong to cold or warm regions respectively, and are plotted in different colours (blue: warm, red: cold). The resulting 3 regimes have been fitted individually, using the ordinary least-squares (OLS) bisector method (dashed lines). The slopes of these lines correspond to dust colour temperatures of 13.9 K, 16.3 K and 19.3 K (see Sect. 3.1). **b** The distribution of the material in the Chamaeleon-Musca using the 3 temperature classes defined by Fig. 1 a. The cold regions are the Chamaeleon main clouds Cha I, Cha II, Cha III. The warm regions on the other hand belong predominantly to the warm near-galactic plane region. Two compact warm sources are seen in Cha I (see text).

UV radiation, e.g. in dense cores, the ISM might cool down to $\approx 10 \text{ K}$ (Krügel & Walmsley 1984; Benson & Myers 1989). Reliable measurements of dust temperatures below 13 K are very rare so far (see eg. Lada et al. 1981). With an ISOSS/IRAS comparison, we can determine dust temperatures down to $\approx 11 \text{ K}$. Below this, $100 \mu\text{m}$ emission becomes too weak (for a typical $170 \mu\text{m}$ -brightness of $\approx 10 \text{ MJy sr}^{-1}$) to be detected by IRAS, and only upper limits for the temperature can be given.

We have started the FIR analysis of cold clouds and cloud cores in Chamaeleon. The Chamaeleon as a test region was chosen for three reasons: (i) because previous molecular line studies revealed dense molecular clouds with and without star formation, (ii) because its ISRF is typical for the solar neighbourhood (i.e. not enhanced locally by massive star formation activity), (iii) because it is only $\approx 150 \text{ pc}$ away (Knude & Høg 1998). At this distance, a typical 1 pc sized molecular cloud and a 0.2 pc sized molecular cloud core have apparent angular diameters of $24'$ and $5'$ respectively, thus can be resolved by ISSA and ISOSS observations.

Previous C^{18}O and ISOPHOT FIR observations of the Cha I cloud (Haikala et al. 1998) revealed cold cores with angular diameters between $4'$ and $10'$, typical $150 \mu\text{m}$ surface brightnesses of $\approx 10 \text{ MJy sr}^{-1}$ and colour temperatures between 13 K and 16 K. All of these cores should be comfortably brighter at $170 \mu\text{m}$ than the confusion limited detection threshold of 2 MJy sr^{-1} found for the Chamaeleon region (see below). The completeness of our search for very cold cores is thus restricted

only in terms of ISOSS sky coverage, which is between 20 % and 30 % for the three Chamaeleon main clouds (even higher in the central parts) and between 10 % and 15 % in the intercloud medium.

This paper locates the regions of lowest FIR colour temperatures in Chamaeleon-Musca. We compare our FIR results with available CO observations and show that the detected cold FIR objects can be identified with dense molecular clouds, and that the cores with lowest colour temperatures are cold in terms of gas temperature too.

2. Observations and data analysis

2.1. The ISOPHOT Serendipity Survey

We have analysed ISOSS data of a $20^\circ \times 20^\circ$ field in Chamaeleon-Musca (see Fig. 1). ISOSS is a far-infrared survey at $170 \mu\text{m}$, using the ISOPHOT C200 detector (Lemke et al. 1996) on board the ISO satellite (Kessler et al. 1996). ISOSS recorded the sky brightness during the slewing of the telescope between two pointed observations. The C200 camera is a 2×2 pixel array with a $3' \times 3'$ field of view. It was used in conjunction with the C_160 broad band filter, which has an effective wavelength of $170 \mu\text{m}$. The fastest read-out rate (1/8 sec) was chosen to achieve a dynamical range of $5 \text{ MJy sr}^{-1} < I_{170} < 500 \text{ MJy sr}^{-1}$. Long slews (exceeding $\approx 2^\circ$) are calibrated using actual detector responsivities, derived from a measurement of the on-board Fine Calibration Source

(FCS) preceding the recording of sky surface brightness. For the remaining slews, default detector responsivities are used. Slews were excluded where one or more detector pixel(s) showed erroneously very high values (“hot pixel”). More details on the measuring mode can be found in Bogun et al. (1996).

Approximately 15 % of the sky is covered with an angular resolution (FWHM) of $\approx 2'$. The in-slew and cross-slew resolutions are similar, since the 1/8 sec on-the-fly integration time corresponds to an in-slew sampling interval of at maximum $1'$. The positional accuracy was determined by comparing positions of point sources with positions of corresponding IRAS sources. An agreement of generally better than $1'$ was found (Stickel et al. 2000). The raw (ERD level) ISOSS data were reduced using a batch processing routine based on the ISOPHOT Interactive Analysis¹ (Gabriel et al. 1997) software package.

The photometric accuracy has been checked in three ways: First, ISOSS results have been compared with dedicated raster maps (mode AOT PHT22), showing an excellent agreement in surface brightness in the Chamaeleon I region. The $18 \times 18 \square'$ sized $100 \mu\text{m}$, $150 \mu\text{m}$ and $200 \mu\text{m}$ maps of Lehtinen et al. (2000) were compared to the ISOSS slewmap. The rms difference between the PHT22 based interpolated $170 \mu\text{m}$ intensity values and the ISOSS intensities is 10 % within the surface brightness range $40 \text{MJy sr}^{-1} - 150 \text{MJy sr}^{-1}$. The gain and the reproducibility uncertainties in the PHT22 absolute photometry itself are 20 % and 6 % respectively (Klaas et al. 1998).

A second check has been made by comparing ISOSS with DIRBE data. We have created interpolated DIRBE $170 \mu\text{m}$ intensities from the $100 \mu\text{m}$, $140 \mu\text{m}$ and $240 \mu\text{m}$ bands, assuming a modified black body spectrum $I_\nu(T) = \text{const.} \cdot \nu^2 B_\nu(T)$ over the whole FIR range. An agreement between ISOSS and DIRBE calibration within 30 % has been found. Finally, the reproducibility of the ISOSS measurements has been tested by evaluating the slew crossing points in several regions. The root mean square of the relative brightness deviation at crossing points is $\lesssim 15 \%$ (slightly dependent on the brightness level).

2.2. Data analysis

Two main approaches were used investigating ISOSS data of a particular region: (1) Building up a map from all measurements along all slews inside the boundaries of the given field, or (2) analysing all individual slews one by one. In our Chamaeleon study, the large scale structures have been investigated using the mapping method (1), the small scale features have been explored analysing each slew individually (2) (see Hotzel et al. 2000).

Both methods make use of the ISSA maps at $100 \mu\text{m}$. In order to achieve absolutely calibrated brightnesses, the ISSA maps were rescaled to agree with the DIRBE calibration: $I_{100} \equiv 0.7 \cdot I_{\nu, \text{ISSA}}(100 \mu\text{m}) + 1.5 \text{MJy sr}^{-1}$. The actual scaling law was

resulted from our comparison of ISSA data with the zodiacal light subtracted DIRBE data of the Chamaeleon-Musca region. They are in accordance with the ISSA – DIRBE transformation found by Wheelock et al. (1994), who however performed an all-sky comparison of the two data sets.

Investigating the large scale structures we have used the whole field of $20^\circ \times 20^\circ$ covering Musca and Chamaeleon to find characteristic FIR colours of the galactic background and of the clouds. About 15 % of this large field and $\approx 25 \%$ of the actual Chamaeleon clouds are covered by ISOSS slews. 64 % of them (accounting for 90 % of the covered area) are calibrated with actual detector responsivities. A composite ISOSS slew map of the region has been produced and has been smoothed to the $5'$ angular resolution of the ISSA maps.

To access the differences in temperature on large spatial scales, we have read out $170 \mu\text{m}$ and $100 \mu\text{m}$ intensities at the slew sample positions from the FIR maps. Their scatter plot (see Fig. 1 a) shows distinct fingers, representing the different temperature regimes. Straight lines have been fitted individually to these fingers, using the ordinary least-squares (OLS) bisector method (see eg. Isobe et al. 1990). The slopes of these lines have been converted to colour temperature in the same way as the I_{170}/I_{100} ratios in the temperature map.

Variation of dust colour temperature was plotted from background corrected $170 \mu\text{m}$ and $100 \mu\text{m}$ intensities. The brightness of the assumed uniform background (20MJy sr^{-1} at $170 \mu\text{m}$ and 8MJy sr^{-1} at $100 \mu\text{m}$) was derived from Fig. 1 a. The ISOSS slew map and the ISSA $100 \mu\text{m}$ maps have been combined to a colour temperature map by assuming modified black body radiation $I_\nu \propto \nu^2 B_\nu(T_d)$ over the whole field, and applying colour corrections for the specific ISOPHOT and IRAS bandpasses. This way we get an overview of the spatial colour temperature distribution of the large grain dust component.

Searching for cold cores the slews are searched individually for sources of high I_{170}/I_{100} ratio as shown in Fig. 2. The ISOSS slews are smoothed to $5'$ to match the IRAS resolution. Doing so, a two-dimensional gaussian smoothing function is centred on the position of the detector centre, thus reducing the data stream to 1 data point per sample (ramp). Corresponding IRAS $100 \mu\text{m}$ intensities are extracted from the ISSA maps using a linear interpolation algorithm. Intensity peaks along the ISOSS slews are located by searching for local maxima in the second derivative of I_{170} as a function of sky position. All peaks exceeding $2 \text{MJy sr}^{-1} (\approx 3\sigma)$ over the background are selected as ISOSS detections. The cross-slew size of a source can not be derived unless it has been crossed by two or more slews. The in-slew size of the source is defined from the I_{170} profile alone, and is assumed to be the same at $100 \mu\text{m}$. For each source, a straight line is fitted to the I_{170} versus I_{100} data points, applying the OLS bisector algorithm. If the variation of background intensity is small and the source is optically thin in the FIR, the fitted line slope reflects the ratio of background corrected intensities. We denote this quantity as *colour parameter* (CP).

¹ The ISOPHOT data presented in this paper was reduced using PIA, which is a joint development by the ESA Astrophysics Division and the ISOPHOT Consortium. The ISOPHOT Consortium is led by the Max-Planck-Institute for Astronomy, Heidelberg.

The colour temperature of the source is derived from CP, assuming modified black body radiation with ν^2 emissivity law, $I_\nu \propto \nu^2 B_\nu(T_d)$, and – again – that the source is optically thin. As before, colour corrections for the ISOPHOT and IRAS band-passes are applied.

Error estimate: The uncertainty of the surface brightness values of individual ISOSS slews is around 20%. The accuracy of the absolute calibration of the IRAS 100 μm values is the same as the DIRBE 100 μm to which it was scaled. According to Hauser et al. (1998) the uncertainty of the DIRBE gain at 100 μm is 13.5%. The derived slopes have an uncertainty of 1% to 19% due to statistical errors. Accordingly we estimate that the total errors of the slopes in Fig 1, and the CP values are 35% to 50%, and thus our 170/100 colour temperatures derived from the scatter plot slopes and CP values have uncertainties of 1.5 K to 2 K.

3. Results

3.1. Dust colour temperature

We can differentiate between regions with different temperatures by their appearance in the ISOSS/IRAS scatter plot (Fig. 1) i.e. by the distance of the corresponding data points to the general correlation line. Data points with $I_{170} > 5 \text{ MJy sr}^{-1}$ above or below this line, (i.e. outside the strip defined by the foreground/background galactic emission) belong to regions with colder or warmer dust respectively. Individual linefits to groups of these outlier points gave slopes of 1.6, 2.6 and 4.5, corresponding to dust colour temperatures of 19.3 K, 16.3 K, and 13.9 K respectively. The lack of a continuous temperature range in the strong FIR emission regime is remarkable. For $I_{100} > 20 \text{ MJy sr}^{-1}$ or $I_{170} > 50 \text{ MJy sr}^{-1}$ there is no indication for colour temperatures in between 16.3 K and 19.3 K. This is an effect of the geometry of the field: Physically separated regions of warm and cold dust are seldom projected onto each other. The bright, compact sources with warm dust discussed below are too small to influence this global picture (see Fig. 1 b). The cold regions are the Chamaeleon main clouds Cha I, Cha II, Cha III. They are projected on the somewhat warmer galactic background. However, for $I_{170} > 50 \text{ MJy sr}^{-1}$ the cold Chamaeleon clouds are dominating the FIR emission. The regions with warm dust ($T(I_{170}/I_{100}) > 19 \text{ K}$) on the other hand belong predominantly to the near-galactic plane region ($|b| < 9^\circ$). Here the line of sight penetrates deeply into the galactic plane, causing intensities $I_{100} > 20 \text{ MJy sr}^{-1}$ and a dominance of the emission from regions with warm dust over the galactic foreground. If the Chamaeleon clouds were projected onto the galactic plane, Fig. 1 a would look different.

The colour temperature map of the central $11^\circ \times 8^\circ$, covering the main clouds Cha I, Cha II and Cha III, is shown in Fig. 3. The whole map shows temperatures below 17 K except for some small warm sources in Cha I (see below). Extended warmer regions are found only in the north east of the large $20^\circ \times 20^\circ$ field (see Fig. 1), i.e. close to the galactic plane.

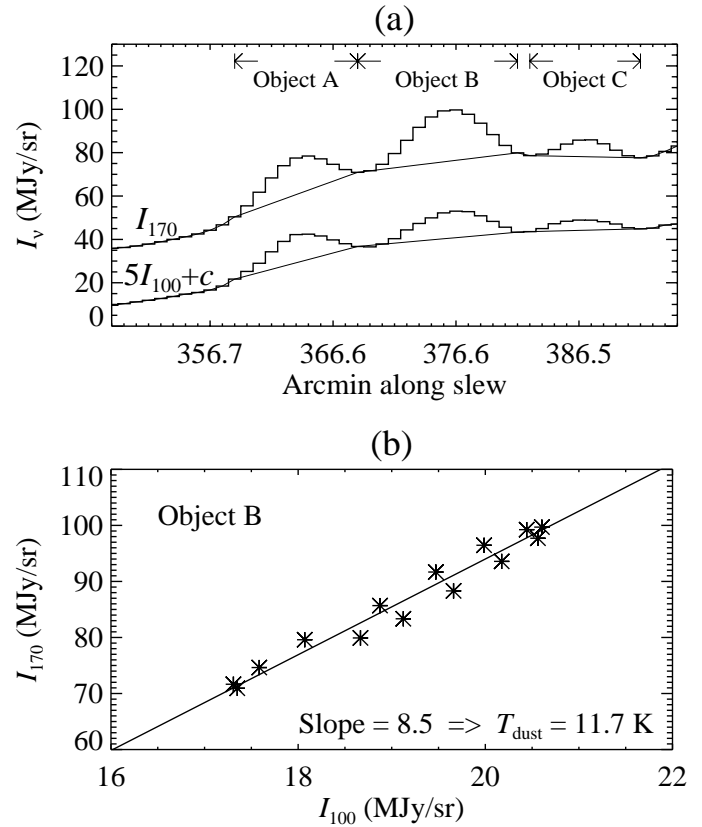


Fig. 2. **a** The IRAS 100 μm and ISOSS 170 μm intensities along a slew crossing Cha I. The ISOSS data are smoothed to match the IRAS resolution. The IRAS 100 μm intensities are scaled by a factor of 5 and a constant is added. Three sources were detected. Peak ‘B’ in the middle is due to VCC no. 4 in Table 1. **b** I_{170} vs. I_{100} plot made with data points towards peak ‘B’. The slope was derived, using the ordinary least-squares (OLS) bisector method. The slope of this line is referred to as CP (colour parameter) which corresponds to dust colour temperature.

Cold dust $\leq 15 \text{ K}$ appears over the whole Cha I cloud (DCld 297.2-15.6), and for the most part of Cha II (DCld 303.0–14.3) and Cha III (DCld 303.0-17.1). The dust of the latter clouds is not quite as cold as in Cha I. While this could be an artefact of a higher galactic background, the cold source search (Sect. 3.2) shows a similar trend, an indication that the subtle temperature differences are real. Cold dust is as well found in G298-13, ($\alpha = 11^{\text{h}}35^{\text{m}}, \delta = -75^\circ 10'$) G295-17 ($\alpha = 10^{\text{h}}21^{\text{m}}, \delta = -77^\circ 30'$), (Boulanger et al. 1998), and in G295-13 ($\alpha = 10^{\text{h}}54^{\text{m}}, \delta = -74^\circ 00'$), the Musca filament, the latter one outside the region of Fig. 3. Altogether, about 3 % of the area measured shows colour temperatures below 15 K.

An $11' \times 7'$ sized warm source is seen in Cha I North at $\alpha = 11^{\text{h}}09^{\text{m}}45^{\text{s}}, \delta = -76^\circ 36'$, with mean brightnesses of $I_{100} = 101 \text{ MJy sr}^{-1}$ and $I_{170} = 164 \text{ MJy sr}^{-1}$. The object is extended perpendicularly to the CO outflow lobes detected by Mattila et al. (1989). It is associated with an $A_V > 15$ mag opaque spot (Jones et al. 1985) and with the bright nebula CED 112 (Cederblad 1946) Another prominent warm source, at $\alpha = 11^{\text{h}}08^{\text{m}}00^{\text{s}}, \delta = -77^\circ 42'$, is associated

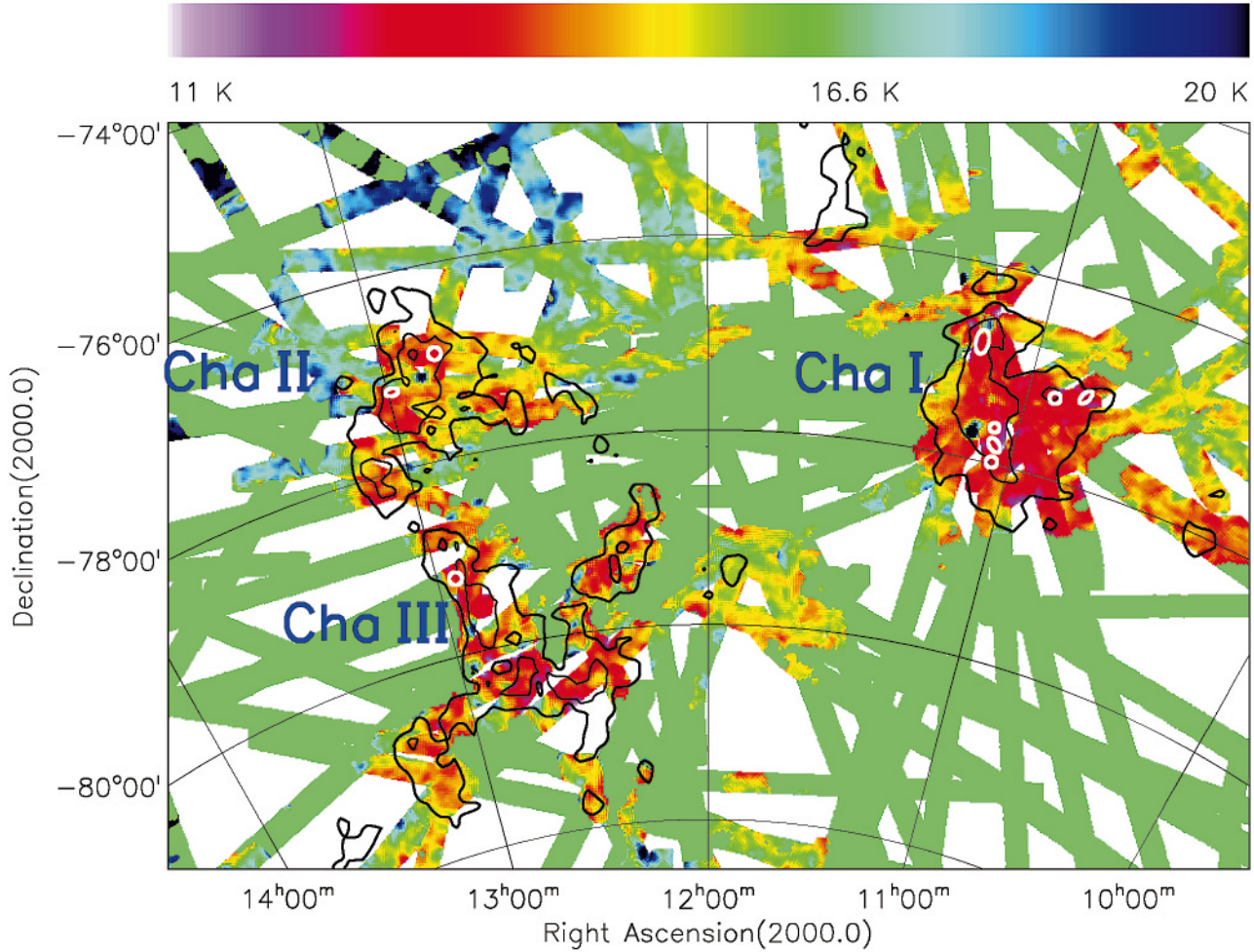


Fig. 3. Dust colour temperature map of the central part of the investigated field, derived from an ISOSS 170 μm slew image and the 100 μm ISSA maps. A FIR background/foreground of 20 MJy sr^{-1} and 8 MJy sr^{-1} respectively was subtracted according to Fig. . 1. The slews are represented by 15' wide stripes, their colors show the colour temperature variation (see bar on top). Overlaid are the contours of the ^{13}CO ($J=1\rightarrow 0$) line intensity at 1.0 K km s^{-1} and 3.5 K km s^{-1} from the survey of Mizuno et al. (1998). Dust colder than 14 K is found only inside the 1.0 K km s^{-1} contour, i.e. is associated with molecular clouds. The small white ellipses indicate the positions of the very cold cores (Sect. 3.2). They are all associated with dense molecular gas (^{13}CO line intensities $> 3.5 \text{ K km s}^{-1}$).

with IRAS 11072-7727 also cited as Chamaeleon Infrared Nebula (Cha IRN) (see Schwartz & Heinze 1983).

3.2. Cold FIR sources

We located 376 ISOSS peaks to be called hereafter *ISOSS sources* and derived their CP colour parameter in the region $\text{RA}=[10^{\text{h}}30^{\text{m}}, 13^{\text{h}}30^{\text{m}}]$ $\text{Dec}=[-82^{\circ}, -75^{\circ}]$ with the following criteria:

- (i) $I_{170}(\text{peak}) > 2 \text{ MJy sr}^{-1}$ (i.e. $> 3 \times \text{rms noise}$),
- (ii) $0 < \text{slope} < 20$ and
- (iii) $\sigma(\text{slope})/\text{slope} < 0.2$ (i.e. a reliable bisector slope).

The size and colour distributions of these 376 ISOSS sources are shown in Fig. 4. The sizes of the ones with $\text{CP} > 7$ are similar to our angular resolution, indicating that most of these objects have a linear size of $\leq 0.1 \text{ pc}$. The colour parameter has an asymmetric distribution. This is partly a result of the method being

designed to find *cold* sources. The distribution has a median of $\text{CP} = 3.8$ and a prominent tail up to $\text{CP} = 9$ corresponding to dust temperatures of 14.5 K and 11.6 K, 86 % of the findings have colour parameters in the range $0 < \text{CP} < 6$, and 7 % of the 376 ISOSS sources have $\text{CP} > 7$. We excluded all the $\text{CP} > 7$ ISOSS sources which were associated by cosmoics or faulty readouts. Also the source position was refined for these very cold ones merging ISOSS sources which were multiple detections of the same object. The ISOSS sources with $\text{CP} < 7$ have not been checked by eye systematically, but only in individual regions of interest (e.g. all the C^{18}O cores discussed in Sect. 4).

The $\text{CP} < 4$ ISOSS sources show a random distribution, while the colder ones cluster at the main clouds Cha I, Cha II and Cha III. There were 28 very cold ISOSS source with $\text{CP} > 7$. Searching for the coldest objects of Chamaeleon we required that $I_{170}(\text{peak})/\text{CP} \geq 1 \text{ MJy sr}^{-1}$ to ensure that the ISOSS

source was detected in $100\ \mu\text{m}$ as well and thus CP reflects a colour temperature. This way we located 6, 2, 1 very cold objects inside the Cha I, Cha II, Cha III molecular clouds respectively. For reasons discussed below, we call these very cold objects *very cold cores* (VCCs). The parameters of the VCCs are listed in Table 1, where the columns are: (1) Core number, for easier identification throughout this paper, (2) ISOSS name, (3–4) equatorial coordinates, (5–7) major and minor diameters and position angle (PA) of the fitted ellipses, (8) colour parameter where the “c” index stands for “confirmed”, (9–10) galactic coordinates, (11) optical association (Hartley et al. 1986). Six of the nine VCCs are double $\text{CP} > 6$ detections, i.e. merged pairs of cold ISOSS sources. The criteria of merging were that the ISOSS sources are closer than $5'$, appearing as crossings of the same IRAS intensity peak. To be classified as a VCC they should have an averaged CP larger than 7. One of the VCCs with “confirmed” CP value is ISOSS 11102–7648 i.e. our VCC no. 7, which was crossed by two slews both showing a $\text{CP} > 7$ source there. These 6 pairs are considered to have a confirmed colour parameter, which we indicate with a “c” index in column (8). The CP values of these cores marked with “c” are more reliable than the rest of the list.

The shape of the cores was determined from the $170\ \mu\text{m}$ profiles and eyeball checks of the $100\ \mu\text{m}$ ISSA maps. These bias effected the values in columns (5–7) mostly for the single detection VCCs: no. 2, no. 6, no. 9. Fig. 5 shows the positions of the very cold objects of Cha I, overlaid on an ISOSS $170\ \mu\text{m}$ slew composite map.

4. Discussion

4.1. Cold dust in molecular clouds

We zoomed to the Chamaeleon part of the Fig. 1 b for a detailed view on the coldest regions and present the colour temperature distribution as derived from the background subtracted I_{170} and I_{100} intensities.

The average intercloud dust colour temperature $T(I_{170}/I_{100})$ in Chamaeleon is 16 K (Figs. 1,3), in between the 17.5 K of galactic cirrus and the 15 K cold dust component derived by Lagache et al. (1998, based on DIRBE I_{240} , I_{140} , I_{100}). The dust of around and below 14 K is strictly concentrated inside the well known molecular clouds and is not found in the diffuse intercloud medium. The average intracloud temperature of Cha I, Cha II and Cha III of 14 K is close to the DIRBE based values of 14.2 K–14.9 K (Boulanger et al. 1998).

Fig. 3 can be used to locate molecular clouds since the regions which show colour temperatures ≤ 15 K are located inside the large CO clouds of Dame et al. (1987) and are associated with ^{13}CO ($J=1\rightarrow 0$) line intensities $\geq 1\ \text{K km s}^{-1}$ (Mizuno et al. 1998, see also contour lines in our Fig. 3). Furthermore, all the cold regions are opaque on the Digitized Sky Survey, with an average extinction of $A_V \approx 2$ mag which is characteristic for molecular clouds.

We have investigated the functional relationship between I_{170} and the visual extinction, using the extinction maps of Cambrésy et al. (1997) and Cambrésy (1999b), which are

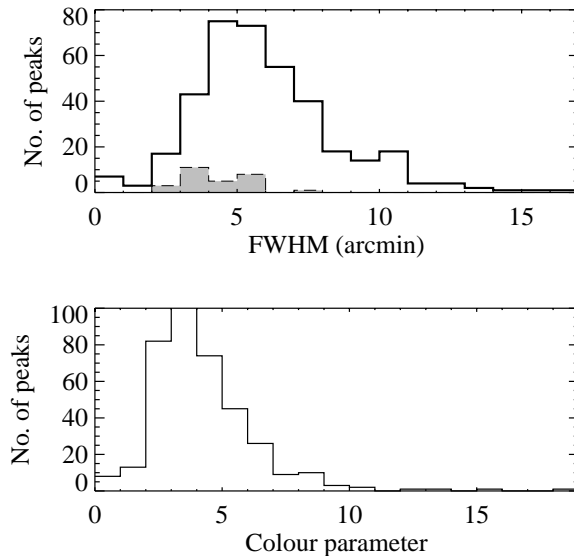


Fig. 4. Full width at half maximum (FWHM) and colour parameter (CP) distributions of the 376 ISOSS sources in Chamaeleon. The FWHM histogram of $\text{CP} > 7$ sources is overlaid with dashed line and shaded. The CP distribution has a median of $\text{CP} = 3.6$ and a prominent tail up to $\text{CP} = 9$, corresponding to dust temperatures of 14.8 K and 11.6 K.

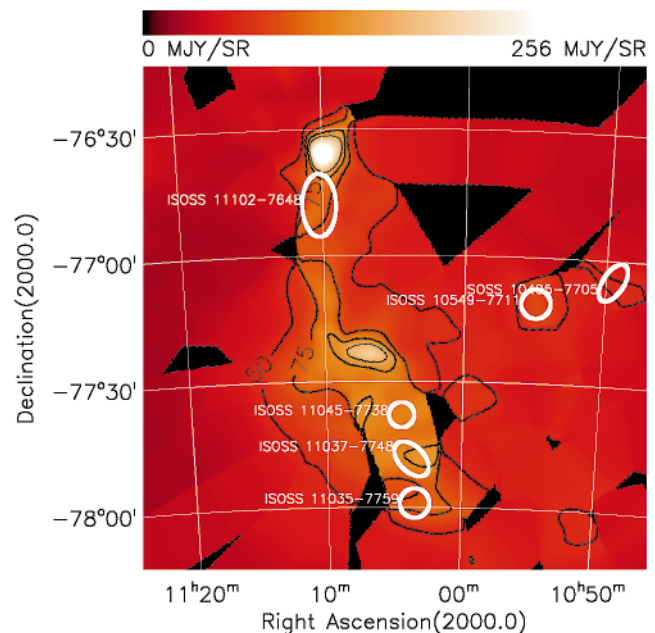
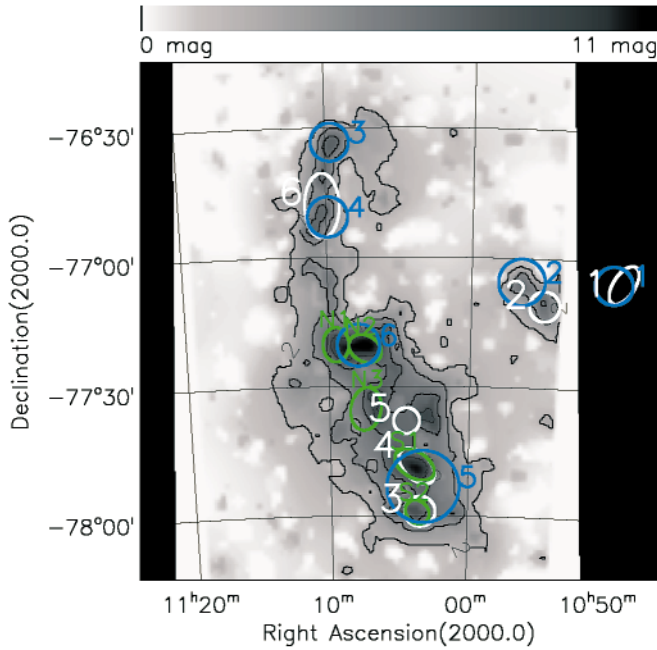


Fig. 5. ISOSS $170\ \mu\text{m}$ slew composite map of Cha I, smoothed to the lower $5'$ IRAS resolution. The intensities are showed for $15'$ wide stripes along slews. Intensities for many interslew positions were interpolated. We note that the actual coverage is about 3 times less than suggested by this smoothed image. Contours are drawn at $I_{170} = 50, 75, 100, 125\ \text{MJy sr}^{-1}$. Overlaid are the positions of the very cold cores, as given in Table 1.

based on J band star counts. We have found that the linear dependence between A_V and I_{170} holds for extinction values up to 7 mag, i.e. I_{170} is an excellent tracer of dust column density as seen in Fig. 7.

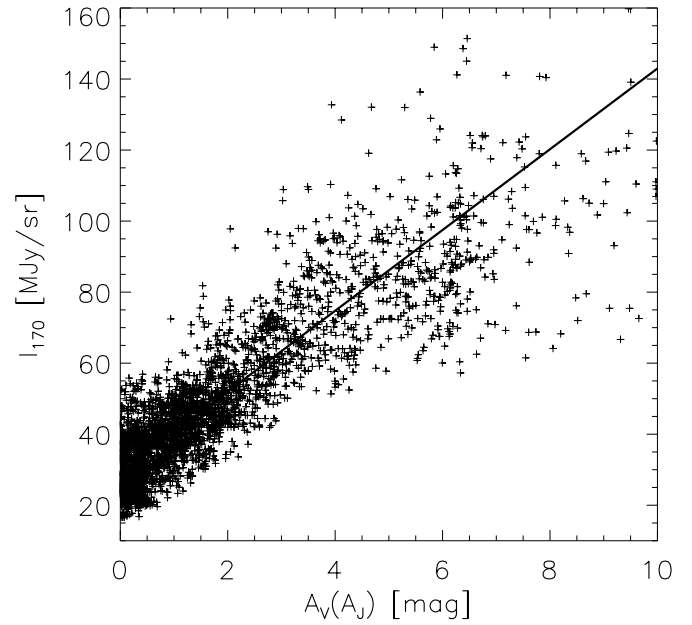
Table 1. Positions and FIR parameters of the very cold cores in Chamaeleon. * PA is the position angle of the major axis, measured anti-clockwise from north through east, “c” marks the CP values based on more than 1 slew measurement.

Core No.	Name	R.A.(2000)	Dec.(2000)	Maj. (arcmin)	Min. (arcmin)	PA* (deg)	CP	l (deg)	b (deg)	Opt. Ass.
(1)	(2)	(3)	(4)	(5)	(6)	(7)	(8)	(9)	(10)	(11)
1	ISSO J10495-7705	10 ^h 49 ^m 30 ^s	−77°05′00″	10	5	150	8.9c	296.162	−15.843	DCld 296.2–15.8
2	ISSO J10549-7711	10 54 55	−77 11 00	7	7	0	8.6	296.488	−15.793	DCld 296.5–15.7
3	ISSO J11035-7759	11 03 30	−77 59 00	7	7	0	7.1c	297.283	−16.312	
4	ISSO J11037-7748	11 03 45	−77 48 30	10	6	45	7.8c	297.219	−16.148	DCld 297.1–16.1
5	ISSO J11045-7738	11 04 30	−77 38 00	6	6	0	8.4	299.488	−15.471	
6	ISSO J11102-7648	11 10 15	−76 48 00	15	8	0	7.3c	297.132	−15.082	DCld 297.2–15.1
7	ISSO J12500-7655	12 50 00	−76 55 00	8	8	0	9.4c	302.848	−14.045	DCld 302.9–14.1
8	ISSO J12560-7913	12 56 00	−79 13 00	8	8	0	7.1	303.341	−16.621	
9	ISSO J12592-7712	12 59 15	−77 12 00	8	5	90	7.5c	303.378	−14.335	DCld 303.5–14.4

**Fig. 6.** The visual extinction in Cha I. The map is based on NIR starcounts and was first shown by Cambrésy et al. (1997). Contours are drawn at $A_V = 2, 4, 6, 8$ mag. The overlaid ellipses are our VCCs (white) and the $C^{18}O$ cores of Haikala et al. (1998) (green) and Mizuno et al. (1999) (blue).

A vivid confirmation of this finding is the remarkable similarity of the morphology of Cha I in I_{170} and A_V (see Figs. 5 and 6).

Boulanger et al. (1998) found in the Chamaeleon main clouds a linear correlation between I_{100} and blue starcount based A_V , which, however, holds for $A_V < 2$ mag only. The better correspondence of I_{170} with A_V as compared to I_{100} is a result of two effects: (i) 170 μ m emission comes from the large grain population only, which is also responsible for the optical extinction, whereas at 100 μ m smaller grains may still contribute. (ii) In high density regions the effective shielding of the ISRF leads to colder dust, which is seen better at the longer wavelength.

**Fig. 7.** $A_V(A_J)$ vs. I_{170} correlation plot for the Cha I region. It shows that the NIR starcount based $A_V(A_J)$ and I_{170} are linearly related in a wide range ($0\text{mag} < A_V(A_J) < 7\text{mag}$), demonstrating how well I_{170} traces the “classical” dust.

As I_{170} measures a single dust component, we have correlated it with the quantity $I_{\text{cold}}(100 \mu\text{m})$ in order to remove contributions from other grain components to the 100 μ m sky brightness. $I_{\text{cold}}(100 \mu\text{m}) = 1.67 \cdot (I_{100} - 5I_{60})$ was introduced by Boulanger et al. (1998) based on Laureijs et al. (1991). It quantifies the excess of $I_L(100 \mu\text{m})$ over $I_L(60 \mu\text{m})$ and was meant to trace the pure cold dust 100 μ m emission on the basis of the IRAS bands. For this purpose, we have extracted 60 μ m ISSA intensities at the same slew positions used already for the I_{170} vs. I_{100} comparison (and scaled similar as before: $I_{60} \equiv 0.8 \cdot I_{\nu, \text{ISSA}}(60 \mu\text{m}) + 1.2 \text{ MJy sr}^{-1}$).

The scatter plot (Fig. 8) reveals a linear correlation between I_{170} and $I_{\text{cold}}(100 \mu\text{m})$. The 30 MJy sr^{-1} offset at the I_{170} -axis is due to the large scale galactic background. The scatter

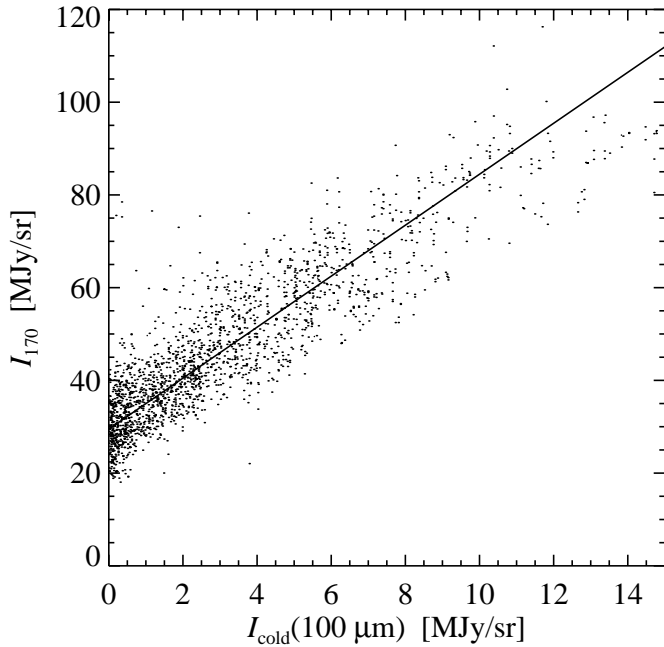


Fig. 8. I_{170} vs. $I_{\text{cold}}(100 \mu\text{m})$ correlation plot for the Chamaeleon region. It shows that the two quantities are linearly related, proving that $I_{\text{cold}}(100 \mu\text{m})$ can be used to trace cold dust. The slope of the fitted line corresponds to the 13.1 K temperature of the cold dust component in the Chamaeleon clouds.

is driven by the temperature variations inside the Chamaeleon clouds due to different degrees of attenuation of the ISRF (e.g. see the VCCs). There is no indication that either of the two quantities is affected by other than the classical dust grain component. This finding justifies the widely used way of locating cold regions by their IRAS based $100 \mu\text{m}$ excess. This is particularly important, as the area filling factor of cold clouds is usually low – in the investigated field only 3%. Therefore one needs the resolution of IRAS to detect this kind of objects.

The slope of the fitted correlation line can be converted to dust colour temperature as in Fig. 1. We have found $T_{\text{dust}} = 13.1 \text{ K}$, which is slightly colder than the 14 K derived in Sect. 3. The small difference may come from different calibration procedures of Boulanger et al. (1998), affecting the conversion factors entering the definition of $I_{\text{cold}}(100 \mu\text{m})$. If the difference is a trace of an I_{100} contamination by other grain components, this effect would in principle also apply to the temperatures of the VCCs (Sect. 4.2). But as the VCCs are not visible in the ISSA $60 \mu\text{m}$ maps, the correction is negligible.

4.2. Very cold cores

Two of the very cold cores (VCCs) are included in the ISOPHOT P22 maps of Lehtinen et al. (2000). See their paper for details on the measurement and calibration. The VCCs no. 3 and no. 4 are both seen on their $18 \times 18 \square'$ sized $100 \mu\text{m}$, $150 \mu\text{m}$ and $200 \mu\text{m}$ maps (see Fig. 9). The background FIR radiation was subtracted using the average brightness of pixels surrounding the ellipse shaped cloud cores. The FIR spectral energy distributions of

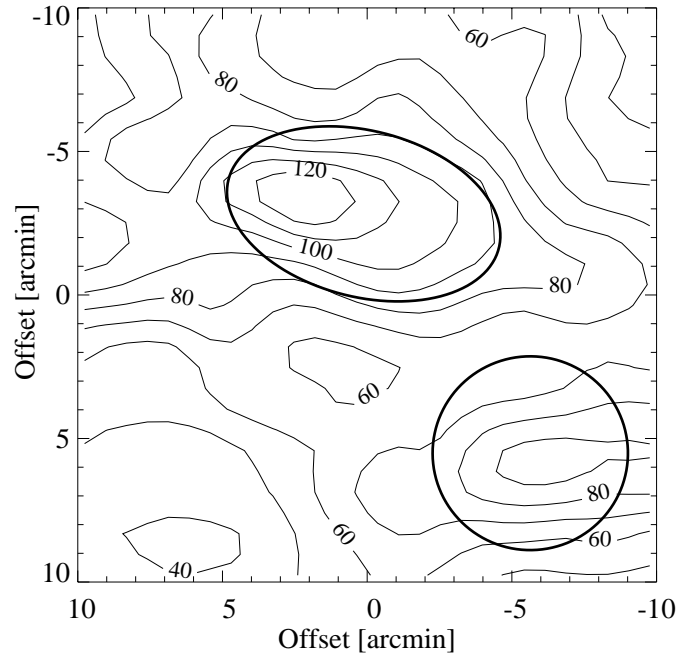


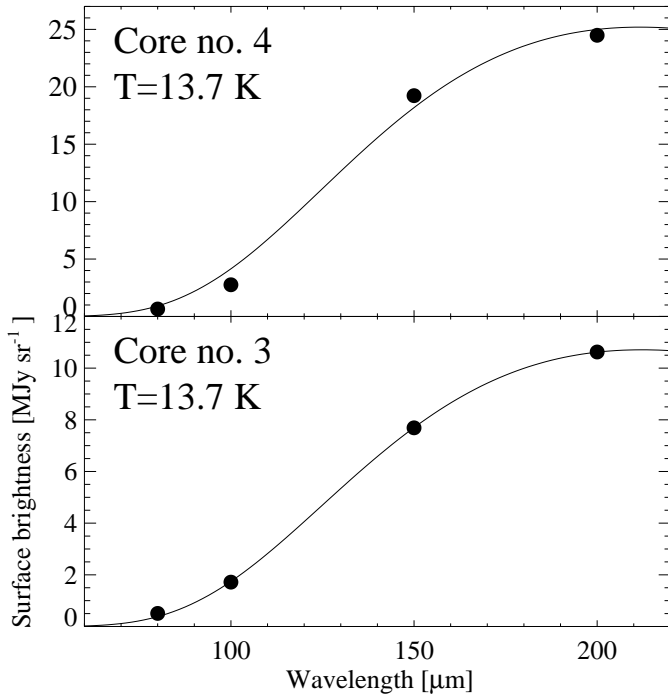
Fig. 9. Contourmap of AOT PHT22 $200 \mu\text{m}$ measurements on the Chamaeleon I south region. Map centre is RA(2000)= $11^{\text{h}}04^{\text{m}}19^{\text{s}}$ Dec(2000)= $-77^{\circ}51'12''$, north is towards the upper left corner. The contours are from 40 MJy sr^{-1} to 120 MJy sr^{-1} in step of 10 MJy sr^{-1} . VCCs no. 3 and no. 4 (see Table 2) are marked with ellipses. Both of them are coinciding with peaks of the $200 \mu\text{m}$ intensity distribution. We note that these are the only cold objects of the field and both were detected by ISOSS as VCCs. See Lehtinen et al. (2000) for details on the PHT22 measurement and calibration.

these cores indicate an absence of warm dust contribution, as it is shown in Fig. 10. The excess surface brightnesses associated with the cores are significantly different but the dust temperatures of the two cores are both $13.7 \pm .5 \text{ K}$. This PHT22 based dust temperature value is similar to the ISOSS results, within the uncertainty limits. It confirms the classification of these cores as cold sources. The position and extent of these VCCs are approved, as well as the fact that they are colder than their surrounding. The difference in the PHT22 and ISOSS based temperature estimates may rise both from the methods deriving the temperature, and the difference in the ways of eliminating the FIR background.

The positions of the VCCs have been compared with visual extinction and C^{18}O data (see Fig. 6). The A_{V} map resolves the internal structure of the cloud, as the near-infrared star count method can trace the visual extinction up to 11 mag. All but one of the VCCs are associated with high extinction peaks ($A_{\text{V}} > 4 \text{ mag}$, see also Table 2). Additionally, all the VCCs lie inside the $W(^{13}\text{CO}) = 3.5 \text{ km s}^{-1}$ contour of the ^{13}CO ($J=1 \rightarrow 0$) line intensity (see Fig. 3 and Mizuno et al. 1998), and associated with $W(\text{C}^{18}\text{O}) \geq 1 \text{ K km s}^{-1}$ C^{18}O line intensity peaks. Hence, our VCCs are indeed opaque, high column density molecular cloud cores. We may assume their line of sight diameters is $\approx 0.2 \text{ pc}$ just as their mean half power diameter is (see Table 1 and the distance), and that half of the observed

Table 2. Physical parameters of the very cold cores. * based on B starcounts (Toriseva & Mattila 1985)

Core No.	Name	A_V (mag)	A_V^{\max} (mag)	T_d (K)	$T_{\text{ex}}(\text{C}^{18}\text{O})$ (K)	$\tau(\text{C}^{18}\text{O})$	$N_{\text{CO}}(\text{H}_2)$ (10^{21} cm^{-2})
(1)	(2)	(3)	(4)	(5)	(6)	(7)	(8)
1	ISOSS 10495-7705	2.0*	3.0*	11.6	–	–	–
2	ISOSS 10549-7711	4.8	6.1	11.7	6.3	0.60	5.2
3	ISOSS 11035-7759	5.0	7.8	12.3	6.4	0.96	11
4	ISOSS 11037-7748	8.0	10.3	12.0	7.3	0.78	12
5	ISOSS 11045-7738	6.8	9.2	11.8	6.2	0.98	16
6	ISOSS 11102-7648	4.7	6.5	12.2	–	< 0.1	(7.6)
7	ISOSS 12500-7655	4.0	5.6	11.5	7.3	0.71	8.3
8	ISOSS 12560-7912	3.0	4.4	12.3	7.0	0.37	3.0
9	ISOSS 12592-7712	8.1	10.4	12.1	8.6	0.31	8.4

**Fig. 10.** Spectral energy distribution of VCCs no. 3 and no. 4 is shown based on ISOPHOT PHT22 images in 80 μm , 100 μm , 150 μm and 200 μm . An emissivity proportional to ν^2 was assumed for the fitted greybody.

C^{18}O column density towards the VCCs is actually by the VCCs itself. The VCC gas densities would then be around $n(\text{H}_2) \approx 10^4 \text{ cm}^{-3}$.

The distribution of dense gas is shown best by Mizuno et al. (1999), who presented full coverage mapping observations of the three Chamaeleon main clouds. We have estimated the physical parameters of the gas associated with the VCCs from their ^{13}CO and C^{18}O spectra by Mizuno (1999), using the measurements nearest to the VCC centres and assuming LTE, thermalised CO, terrestrial isotopic ratios, and $N(\text{H}_2) = 2 \times 10^5 N(^{13}\text{CO})$.

The dust and gas parameters are compared in Table 2, where the columns are: (1) Running number as in Table 1, (2) ISOSS name, (3–4) average and peak visual extinction

(Cambr sy et al. 1997; Cambr sy 1999b), (5) dust colour temperature, derived from column 8 of Table 1, errors in T_d are 1–2 K (6) C^{18}O excitation temperature, (7) optical depth of C^{18}O (at line centre), (8) H_2 column density, derived from C^{18}O .

Seven of the nine VCCs have been found cold with $T_{\text{ex}}(\text{C}^{18}\text{O}) = 7.4 \text{ K} \pm 1.2 \text{ K}$. However, $T_{\text{ex}}(\text{C}^{18}\text{O})$ can provide only a first order estimate of the kinetic temperature, since C^{18}O is expected to be sub-thermal in dense cores. NH_3 is a better indicator of gas temperatures in dense cores. An ammonia survey of the VCCs would thus be necessary to confirm the low gas kinetic temperatures.

A general correlation is not expected between gas temperature and colour temperature of large dust grains. The heating and cooling mechanisms are different. Gas – dust interactions play a dominant role in the thermal balance only at high densities, and gas – dust encounters are most frequent between molecules and the more abundant smaller dust grains. Both gas and dust might, however, cool down below 15 K already at moderately high densities of $n(\text{H}_2) \approx 10^4 \text{ cm}^{-3}$ when the incident flux is low (Kr gel & Walmsley 1984). We claim that this is the case in the dense parts of the Chamaeleon clouds, where the shielding from the outside radiation field is effective and the star forming regions do not form massive stars. The radiation from the low mass stars heats the ISM only in their vicinity.

The very cold cores have very low gas temperatures as it is seen from molecular line measurements (Table 2). To compare with the calculations of Kr gel & Walmsley (1984) we assume that the mean intensity of the ISRF impinging at the Chamaeleon VCCs is one third of the mean ISRF in the solar neighbourhood i.e. $2.67 \times 10^{-2} \text{ erg cm}^{-2} \text{ s}^{-1}$ (Metzger 1990), and that the UV radiation of hot stars and HII regions is effectively shielded by the ISM into which the VCCs are embedded. Thus we assume a soft radiation field ($T_r = 3000 \text{ K}$) with low incident flux of $F \approx 10^{-2} \text{ erg cm}^{-2} \text{ s}^{-1}$. For such a radiation field, a grain size distribution $n(a) \propto a^{-3.5}$ (Mathis et al. 1977), and a gas density of the order 10^4 cm^{-3} Kr gel & Walmsley (1984) calculated gas and dust temperatures of $\approx 8 \text{ K}$ and $\approx 12 \text{ K}$ respectively which are in the range we found for our VCCs. Hence, we regard our method for finding very cold FIR sources as an effective way to locate the coldest cloud cores in terms of gas temperature, too.

4.3. Completeness and reliability of the cold source search

The C¹⁸O survey of Mizuno et al. (1999) fully covers the three Chamaeleon main clouds with an angular resolution (2.7') similar to ours. We have therefore used their list of 23 C¹⁸O cores to investigate the completeness of our method to locate cold cloud cores: 15 of the 23 cores have been crossed by ISOSS slews. All these 15 cores have been detected. 11 (73 %) are cold with $T_{\text{dust}} \leq 15$ K, 6 (40 %) are associated with VCCs.

The characteristics of the C¹⁸O cores differ in the three clouds. We therefore compare the gas and dust properties in the most densely covered Chamaeleon I region, where all six C¹⁸O cores have been crossed by ISOSS slews: The C¹⁸O cores no. 1, 2 and 4 have been identified as VCCs no. 1, 2 and 6, respectively. C¹⁸O core no. 5 contains the two separated VCCs no. 3 and 4 (Fig. 6).

While the four C¹⁸O cores of Chamaeleon I associated with VCCs have colour temperatures < 13 K (Table 2) and C¹⁸O core no. 6 is associated with sources of $T_{\text{dust}} \approx 14.5$ K, C¹⁸O core no. 3 has $T_{\text{dust}} \approx 20$ K (warm sources are not indicated in the Figs. 5 and 6). This core, which contains much warmer dust than all others, is seen towards a peak in surface density of young stellar objects.

4.4. Two sources of Cha I with warm dust

In this paper we have not intended to test the capabilities of the ISOSS/IRAS analysis studying the dust in warm regions. The two warm sources seen in Cha I are both heated internally by embedded young stellar objects. CED 112 is at the southern edge of a group of pre-main-sequence stars (North et al. 1996) with mid-infrared excess (Persi et al. 2000). The bipolar nebula Cha IRN was classified by Ageorges et al. (1996) as a free-falling cloud molecular core with bipolar outflow cavities and embedded young star-disk system. Cohen & Schwartz (1984), using KAO FIR measurements with effective FWHM beam-sizes of about 45'' derived 65 K as the temperature of the coldest dust component seen there. The fluxes of these warm spots are mainly caused by point sources. The colour temperatures derived from our 5' angular resolution ISOSS/IRAS data (24 K and 19 K respectively) are due to a mixture of radiation of circumstellar and interstellar dust seen in the beam with various temperatures. The physics of large dust particles in heated environment can be studied by ISOSS at regions where external heating is dominant, i.e. the heating source can be separated with our resolution.

5. Conclusion and outlook

The combined ISOSS 170 μm and IRAS 100 μm data sets are a useful tool to characterize cold dust in galactic molecular clouds and to find cloud cores with very low FIR colour temperatures. The main findings of our investigation in the test region Chamaeleon are as follows:

- The dust colour temperature is ≈ 16 K for the intercloud medium and around 14 K inside the ¹³CO clouds.

- The comparison of 170 μm emission with optical extinction has shown a linear correlation up to $A_V \approx 7$ mag. This qualifies I_{170} as a good tracer of dust column density.
- We have found $I_{\text{cold}}(100 \mu\text{m})$ (Boulanger et al. 1998) well correlated with I_{170} , which finally proves the assumption that combined IRAS 60 μm and 100 μm bands can be used to locate clouds with cold dust.
- We have developed a method for finding very cold cores, and located 9 VCCs. Comparison of our VCCs with earlier near infrared and CO surveys has proven that these objects are indeed highly opaque molecular cloud cores.
- The VCCs have high gas column densities and low CO excitation temperatures, $T_{\text{ex}}(\text{C}^{18}\text{O}) \approx 8$ K.
- The physical parameters of the very cold cores agree with the results of radiative transfer calculations for a spherical model cloud heated from outside by one third of the ISRF at the solar neighbourhood.

The sample we will obtain analysing the complete ISOSS database (≈ 15 % of the sky) is much larger than any of the previous FIR samples. The very cold core search will be extended to the giant molecular cloud complexes in Orion, Taurus, Cepheus, Cygnus and Ophiuchus. Extrapolating the results of our Chamaeleon survey, we expect to detect more than a hundred very cold cloud cores in the Milky Way. A series of follow-up measurements in cm, mm and sub-mm wavelengths has been started in order to derive the physical properties of the gas in the very cold cores.

Acknowledgement. We acknowledge the valuable comments by the referee.

The ISOPHOT project and Post-operation Phase was funded by the Deutsches Zentrum für Luft- und Raumfahrt (DLR, former DARA), the Max-Planck-Gesellschaft, the Danish, British and Spanish Space Agencies and several European and American institutes.

Members of the Consortium on the ISOPHOT Serendipity Survey (CISS) are MPIA Heidelberg, ESA ISO SOC Villafraanca, AIP Potsdam, IPAC Pasadena, Imperial College, London.

L.V. Tóth acknowledges an MPI research fellow grant. This research was partly supported by the OTKA grants F-022566 and T-024027 and the JSPS-HAS Cooperative Science program No. 18. The work of K.L. and K.M. has been supported by the Academy of Finland through grant No. 1011055.

This research has made use of the Digitized Sky Survey, produced at the Space Telescope Science Institute, NASA's Astrophysics Data System Abstract Service, the Simbad Database, operated at CDS, Strasbourg, France, and the NASA/IPAC Extragalactic Database (NED), which is operated by the Jet Propulsion Laboratory, California Institute of Technology, under contract to the National Aeronautics and Space Administration.

K.L. and K.M. thank Carlos Gabriel (ISO Data Centre, Villafraanca) for providing them with the IDL runtime version of PIA.

References

- Ageorges, N., Fischer, O., Stecklum B., et al., 1996, ApJ, 463, L101.
 Benson, P.J., Myers, P.C., 1989, ApJS, 71, 89.
 Bogun S., Lemke D., Klaas U., et al., 1996, A&A 315, L71

- Boulanger F., Bronfman L., Dame T.M., et al., 1998, *A&A* 332, 273
- Cambrésy L., 1999a, *A&A* 345, 965
- Cambrésy L., 1999b. Etude de l'extinction et de la formation stellaire dans les nuages moléculaires à l'aide de données des domaines infrarouge (DENIS) et optique (USNO). Ph.D. thesis, Université Paris 7
- Cambrésy L., Epchtein N., Copet E., et al., 1997, *A&A* 324, L5
- Cederblad, S., 1946, *MeLu*, II, 119, 1.
- Cohen M., Schwartz R.D., 1984, *AJ*, 89, 277.
- Dame T.M., Ungerechts H., Cohen R.S., et al., 1987, *ApJ* 322, 706
- Draine B.T., Lee H.M., 1984, *ApJ* 285, 89
- Gabriel C., Acosta-Pulido J., Heinrichsen I., et al., 1997, The ISOPHOT Interactive Analysis PIA, a Calibration and Scientific Analysis Tool. In: Hunt G., Payne H.E. (eds.), *ASP Conf. Ser. 125: Astronomical Data Analysis Software and Systems VI*, vol. 6, p. 108
- Haikala L.K., Mattila K., Lehtinen K., et al., 1998, ISOPHOT FIR and SEST Molecular Line Mapping of Chameleon I. In: Yun J.L., Liseau R. (eds.) *ASP Conf. Ser. 132: Star Formation with the Infrared Space Observatory*, p. 147
- Hartley M., Tritton S.B., Manchester R.N., et al., 1986, *A&AS* 63, 27
- Hauser M.G., Arendt R.G, Kelsall T., 1998, *ApJ* 508, 25.
- Hotzel S., Lemke D., Krause, O., et al., 2000, *Lecture Notes in Physics*, 548, 259
- Isobe T., Feigelson E.D., Akritas M.G., Babu G.J., 1990, *ApJ* 364, 104
- Jones T.J., Hyland A.R., Harvey P.M., et al., 1985, *AJ* 90, 1191
- Keene J., 1981, *ApJ* 245, 115
- Kessler M.F., Steinz J.A., Anderegg M.E., et al., 1996, *A&A* 315, L27
- Klaas U., Laureijs R.J., Radovich M., et al., 1998, ISOPHOT Calibration Accuracies. SAI/98-092/Dc Version 2, ESA
- Knude J., Høg E., 1998, *A&A* 338, 897
- Krügel E., Walmsley C.M., 1984, *A&A* 130, 5
- Lada C.J., Thronson, H. A., Jr.; Smith, H. A. et al., 1981, *ApJ* 251, L91
- Lagache G., Abergel A., Boulanger F., et al., 1998, *A&A* 333, 709
- Launhardt R., Ward-Thompson D., Henning T., 1997, *MNRAS* 288, L45
- Laureijs R.J., Clark F.O. Prusti T., 1991, *ApJ* 372, 185.
- Lehtinen K., Haikala L.C., Mattila K., Lemke D., 2001, *A&A*, in press
- Lemke D., Klaas U., Abolins J., et al., 1996, *A&A* 315, L64
- Mathis J.S., Rumpl W., Nordsieck K.H., 1977, *ApJ* 217, 425
- Mattila K., Liljeström T., Toriseva M., 1989, Recent Observations with SEST of the Starforming Cloud Epsilon-Chamaeleontis-I. In: Reipurth B. (ed.) *Proc. ESO Workshop: Low Mass Star Formation and Pre-Main-Sequence Objects*, ESO, p. 153
- Metzger P.G., 1990, The Interstellar Radiation Field and its Interaction with the Interstellar Matter In: Bowyer S., Leinert Ch., (eds.) "The Galactic and extragalactic background radiation", Kluwer, p. 63
- Mizuno A., 1999, private communication
- Mizuno A., Hayakawa T., Yamaguchi N., et al., 1998, *ApJ Lett.* 507, L83
- Mizuno A. Hayakawa T., Tachihara K., Onishi T., et al., 1999, *PASJ* 51, 859.
- North L., Olofsson G., Abergel A., et al., 1996, *A&A*, 315, 185.
- Persi P., Marenzi A.R., Olofsson G., et al., 2000, *A&A*, 357, 219.
- Ristorcelli I., Serra G., Lamarre J.M., et al., 1998, *ApJ* 496, 267
- Schwartz, R.D., Heinze, K.G., 1983, *AJ*, 88, 1665.
- Stickel M., Bogun S., Lemke D., et al., 1998a, *A&A* 336, 116
- Stickel M., Lemke D., Bogun S., et al., 1998b, *Proceedings of SPIE* 3349, 115
- Stickel M., Lemke D., Klaas U., et al., 2000, *A&A*, 359, 865.
- Toriseva M., Mattila K., 1985, *A&A*, 153, 207.
- Wheelock S.L., Gautier T.N., Chillemi J., et al., 1994, IRAS sky survey atlas: Explanatory supplement. JPL Publication 94-11, IPAC, JPL